sustainability

MDPI

Article

Natural Fractures and Their Contribution to Natural Gas Migration and Accumulation in Marine Carbonate Reservoirs: Lower Triassic Feixianguan Formation, Northeast Sichuan Basin, China

Cong Guan [1,2], Lianbo Zeng [1,2,*], Yingtao Yao [1,2], Hang Zhang [3], Jiewei Zhang [3] and Dong Liang [1,2]

[1] National Key Laboratory of Petroleum Resources and Engineering, China University of Petroleum (Beijing), Beijing 102249, China; conggcup@163.com (C.G.); 2020310032@student.cup.edu.cn (Y.Y.); dong_liangg@163.com (D.L.)
[2] College of Geoscience, China University of Petroleum (Beijing), Beijing 102249, China
[3] Northeastern Sichuan Oil and Gas District, PetroChina Southwest Oil and Gas Field Company, Dazhou 635000, China; zhanghang@petrochina.com.cn (H.Z.); zhangjiewei@petrochina.com.cn (J.Z.)
* Correspondence: lbzeng@sina.com

Abstract: The Lower Triassic carbonate succession of the Feixianguan Formation represents a primary focus for gas exploration in the northwestern Sichuan Basin. This study area includes the massive Puguang gas field and other nearby gas fields of considerable size. These carbonate reservoirs display significant heterogeneity, which is primarily influenced by the presence of natural fractures. Extensive documentation of fracture types, characteristics, effectiveness, and their role in enhancing reservoir properties was conducted by examining and analyzing various data sources, including cores, thin sections, image logs, and experimental measurements. Shear fractures primarily characterize the Feixianguan Formation carbonate reservoir, although tensile and diagenetic fractures are also present, albeit in fewer numbers. Tectonic fractures are the dominant type, particularly unfilled ones with dip angles greater than 60° in the NEE–SWW direction. These fractures are mainly filled with calcite. The tectonic fractures were formed in three stages: Late Indosinian-Early Yanshanian, Late Yanshanian-Early Himalayan, and Late Himalayan. These fractures intersect with the in situ stress direction at a small angle in the NE–SW, NEE–SWW, and near E–W directions, contributing to their effectiveness. Compared with the total fracture density, the effective fracture density is the factor in controlling gas production. An increase in the proportion of effective fractures tends to result in a rise in gas productivity. Additionally, the orientation of effective fractures also influences natural gas production. Fractures striking in the E–W and NE–SW directions, which are particularly effective, are associated with high natural gas production.

Keywords: tectonic fractures; fracture characteristics; effectiveness; carbonate reservoir; Sichuan Basin

Citation: Guan, C.; Zeng, L.; Yao, Y.; Zhang, H.; Zhang, J.; Liang, D. Natural Fractures and Their Contribution to Natural Gas Migration and Accumulation in Marine Carbonate Reservoirs: Lower Triassic Feixianguan Formation, Northeast Sichuan Basin, China. *Sustainability* **2023**, *15*, 16155. https://doi.org/10.3390/su152316155

Academic Editor: Hariklia D. Skilodimou

Received: 23 August 2023
Revised: 23 October 2023
Accepted: 13 November 2023
Published: 21 November 2023

1. Introduction

Marine carbonate successions are crucial targets for oil and gas exploration, given their substantial contribution to global hydrocarbon reserves [1–4]. However, the exploration and production efforts are challenged by the presence and distribution of natural fractures in carbonate rocks [5–7]. Previous studies have indicated that after diagenetic transformations, primary pores in carbonate reservoirs decrease, making secondary pores and fractures the dominant factors governing reservoir spaces [8,9]. Tectonic and diagenetic processes lead to the development of natural fractures in deep-buried carbonate reservoirs. These fractures contribute to significant reservoir heterogeneity [10,11]. Natural fractures play a crucial role in determining reservoir quality by providing storage space for hydrocarbons and serving as conduits for fluid migration and flow [12]. Additionally, fractures of different scales can connect pores, influencing the reservoir's petrophysical properties [13]. Understanding

the characteristics of natural fractures and their impact on reservoir properties is essential for evaluating and predicting high-quality reservoirs. Such understanding is crucial for successfully exploring and developing carbonate reservoirs [14–16].

Scholars have gathered a wealth of experimental and observational data through field observations, geological surveys, geophysical exploration, laboratory experiments, analog modeling, and numerical simulations [17–19], which has led to the proposal of influential theoretical models and explanations. These methods have been used for extensive studies on the types, characteristics, controlling factors, and the formation and evolution of natural fractures [1,5–9]. However, the strong heterogeneity of carbonate rocks obscures the clear understanding of the influence of natural fractures on the production of carbonate reservoirs [20,21]. Recently, significant gas fields, including Puguang, Luojiazhai, Yuanba, and Qilibei, have been discovered in the Changxing-Feixianguan Formation located in the northeastern Sichuan Basin [22,23]. These formations primarily consist of grain shoal carbonate reservoirs, predominantly dolomite in lithology, with storage space comprising dissolution pores, intercrystalline pores, and fractures [22–24]. However, previous research mainly focused on sedimentary evolution, diagenesis and reservoir characterization, hydrocarbon generation mechanisms, and reservoir adjustment processes in northeastern Sichuan [25–27].

Studies on natural fractures have been ignored [26], leading to incomplete and limited research on related fractures. However, cores from gas fields such as Puguang, Tieshanpo, and Yuanba have shown the widespread distribution of fractures, as well as phenomena of dissolution enlargement and bitumen fillings along fractures [25,28,29]; these findings confirm that fractures serve as significant storage spaces and fluid flow channels in the northeastern Sichuan Basin [30–32]. Exploratory studies have demonstrated a close relationship between gas production and the extent of fracture development in northeastern Sichuan [20,31,33]. Despite the high prevalence of fractures observed in the Feixianguan Formation, the mechanism behind their formation remains elusive. This lack of understanding impedes comprehension of the relationship between fractures and hydrocarbon accumulation and hinders the establishment of accurate geological models.

In this study, we employed core data, thin sections, and scanning electron microscopy to identify types of natural fractures. We combined these methods with image logs to examine the characteristics of natural fractures, including fracture density, fracture strike, fracture dip angle, and fracture filling degree within the Feixianguan formation. Additionally, we used the cross-cutting relationship between fractures and the homogenization temperature of fluid inclusions within the calcite cement to analyze the timing of fracture formation. Based on the collected data, we investigated the effectiveness of natural fractures in different directions and their influence on oil and gas production, and ultimately analyzed the contribution of natural fractures to productivity. The findings of this study hold significant implications for guiding the exploration and development of shoal-type carbonate reservoirs. In addition, compared to coal and oil, natural gas combustion produces less carbon dioxide and air pollutants, reducing environmental pollution and climate change impacts. Natural gas also can play a crucial role as a transitional energy source during the energy transition process. It can help reduce reliance on coal while providing a stable supply for the development of renewable energy sources.

2. Geological Setting

The Sichuan Basin, covering an area of approximately 180,000 km^2, is a vast superimposed basin. The study area is in the northeastern part of the Sichuan Basin in China (Figure 1). The Sichuan Basin covers an area of approximately 180,000 km^2. The study area under consideration is situated in the northeastern part of the Sichuan Basin in China (Figure 1a) [26,34]. From the Late Permian to the Early Triassic period, the study area has undergone a series of intricate tectonic events, including the Indonesian, Yanshanian, and Himalayan movements, which have led to the development of faults and folds [26,35].

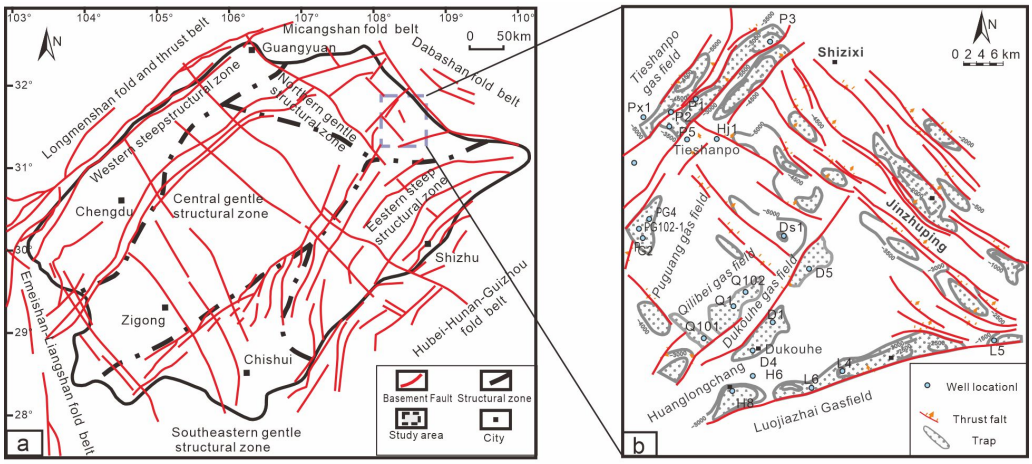

Figure 1. The basement faults distribution and location of the study area (modified from [34]). (**a**) Tectonic map of Sichuan Basin. (**b**) Distribution of traps and faults in the study area.

The Feixianguan Formation in northeastern Sichuan is a platform carbonate succession with a thickness ranging from 445 m to 720 m. The reservoir lithology in this area is primarily composed of grain dolomite, crystalline dolomite, and oolitic limestone [36]. The sedimentary facies within the formation include carbonate ramp subfacies, platform margin subfacies, open platform subfacies, and evaporative carbonate platform subfacies. The reservoirs are mainly developed in the shoals of the platform margin and open platform subfacies [37]. Owing to the diagenetic transformation, the primary pores in the Feixianguan Formation have undergone dissolution, making them difficult to identify. As a result, the reservoir space in this formation mainly consists of secondary dissolutive pores, intercrystalline pores, and fractures. When fractures occur in the Feixianguan Formation, there is a notable difference in reservoir quality. The porosity difference between the maximum and minimum values can be as high as one order of magnitude, while the permeability difference can be as high as three orders of magnitude.

3. Data and Methods

Our observations are derived from analyzing carbonate reservoirs within the Lower Triassic Feixianguan Formation in the northeast Sichuan Basin. The data used in this study comprise 1420 m of cores from 17 wells and borehole image logs from 12 wells. To determine the microscopic characteristics and formation time of the natural fractures, we collected 142 carbonate samples. These samples underwent microscopic identification, scanning electron microscope (SEM) analysis, and fluid inclusion experiments.

The attributes of fractures, as derived from cores and borehole image logs, encompass parameters such as strike, dip angle, density, and filling conditions. It is worth noting that in this study, the parameter used to measure fracture density is linear density. Linear density is computed by determining the number of fractures per unit length (Figure 2), as observed in cores [38,39]. However, it is crucial to acknowledge the potential for sampling bias as the apparent fracture density derived from vertical well cores may not accurately represent the true subsurface parameters. To obtain the true linear density, the number of fractures per unit length along the normal direction to the fracture planes was recalculated using the following formula:

$$\rho = \frac{n}{L|\cos(\theta + \alpha)|}$$

ρ refers to true linear density ($m - 1$), n represents the number of fractures counted on cores, L refers to the core length in statistics (m), θ is the dip angle of fractures (°), and α is well deviation angle.

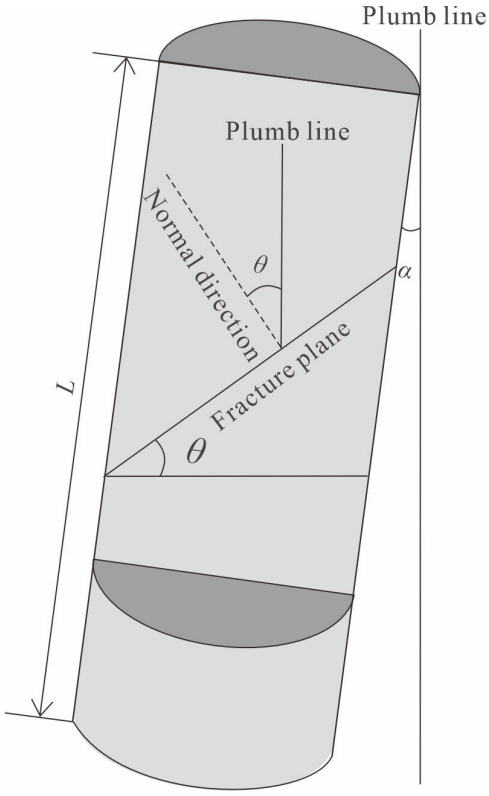

Figure 2. Schematic diagram of calculation model of fracture linear density. *L* refers to the core length in statistics (m), θ is the dip angle of fractures (°), and α is well deviation angle.

It is essential to highlight that the microscopic fractures scrutinized in this study bear a resemblance to the matrix pores, observable solely through the use of an optical microscope, whereas large-scale fractures were discerned on cores with unaided vision. To assess fracture distribution accurately, 117 thin sections were prepared and stained with Alizarin Red-S and potassium ferricyanide [40]. The FEI Quanta 200 F scanning electron microscope (SEM) also analyzed five core sample fragments.

When the inclusions undergo artificial heating at room temperature, their phase state alters with the temperature rise. Upon reaching a specific temperature, the multiphase state vanishes and the inclusions revert to their initial single-phase fluid state. This temperature, at which the phase transition occurs, is referred to as the homogenization temperature [41]. The temperature preserved in the fluid inclusions can be obtained to ascertain the stages of fracture formation. To measure the temperatures of fluid inclusions, fifteen thin sections of fracture fillings of varying depths were prepared.

The study emphasized selectively measuring the fluid inclusions within the filling minerals close to the fracture walls. This approach was designed to provide insights into the approximate time of fracture formation, inferred from the mineral filling time. The inclusion of thin sections used in this study measured approximately 40 mm × 20 mm, with a uniform thickness of 0.1~0.3 mm. These thin sections were bonded with fir glue and slides.

The petrography analysis of the fluid inclusions was initially conducted using a Leica DM4500 microscope, enabling the identification of distinct fluid inclusion assemblages (FIA). Subsequently, micro thermometry was performed on the aqueous fluid inclusions utilizing a Linkam THMS600 hot and cold platform. The homogenization temperatures (Th) and final melting temperatures (Tm) of 72 aqueous fluid inclusions were meticulously determined and calibrated, employing the well-established methodologies described by Goldstein and Reynolds (1994) [42]. The temperature uncertainties associated with the measurements were quantified as ±1 °C for Th and ±0.1 °C for Tm, respectively. The

heating rate was maintained at 0.1–5.0 °C/min and the temperatures at which the inclusions were fully homogenized and completely dissolved were observed and documented during the microscopic temperature measurement of the fluid inclusions (Figure 3).

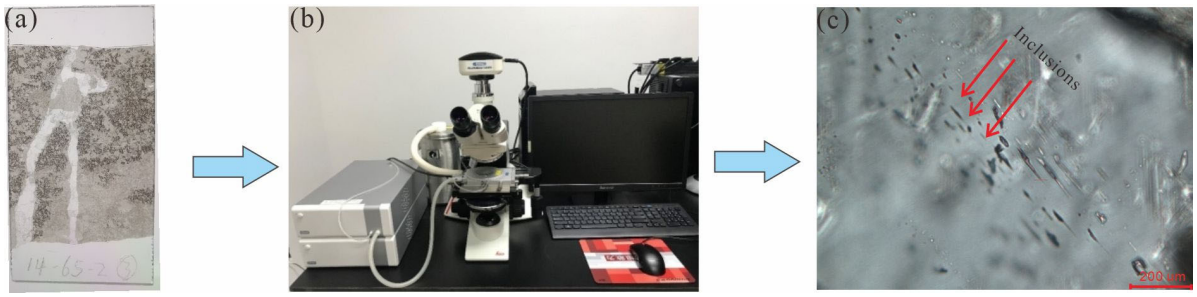

Figure 3. Fluid inclusion test process. (**a**) Preparation of fluid inclusion samples. (**b**) Instruments for observation and temperature measurement of fluid inclusions made in Linkam Scientific Instruments Limited in Salfords, UK. (**c**) Observation results and acquisition of homogenization temperature of fluid inclusions.

4. Results

4.1. Types of Natural Fractures

The Feixianguan Formation in the study area has undergone numerous tectonic shifts and complex diagenetic processes, resulting in various natural fractures. These fractures can be divided into two types according to their formation mechanisms: tectonic and diagenetic.

Tectonic fractures can be further classified into two subtypes based on their formation stress state: shear fractures and tensile fractures. Shear fractures tend to occur in groups and exhibit stable extensional characteristics (Figures 4a–d and 5g). The fractures within the same group are often arranged in echelon patterns (Figure 4b) and possess relatively flat fracture surfaces with developed scratches (Figure 4c). Different groups of fractures intersect (Figure 5e) and some core samples exhibit conjugate shear fractures (Figure 4e). Tensile fractures occur sporadically, have limited extension, rough fracture surfaces, lack slickensides, and show uneven fracture widths (Figure 4g).

Diagenetic fractures, including stylolites, bedding, and dissolution fractures, are formed due to diagenesis-related processes. Stylolites commonly found in carbonate rocks, particularly at lithological transition interfaces, are associated with pressure solution processes. While most stylolites develop nearly horizontally, some may exhibit inclined or vertical orientations (Figure 4f,i). The planes of stylolites are usually enriched with black insoluble residues (Figure 4f). Bedding fractures occur along sedimentary bedding planes. Their fracture surfaces appear relatively irregular and may exhibit a discontinuous distribution pattern. These fractures typically follow the bedding planes and are observed to occur at evenly spaced intervals.

It should be noted that bedding fractures are rarely filled with materials (Figure 4h). Dissolution fractures are formed through the dissolution process without any structural rupture. These fractures result from the enlargement of irregular secondary dissolution pores, which are initially created by dissolution. Over time, these pores may expand, forming dissolution grikes and, ultimately, fractures. Dissolution fractures exhibit irregular shapes, often appearing as serpentine, harbor-shaped, branching, or funnel-shaped forms (Figure 5c). The surfaces of dissolution fractures are generally rough and uneven, exhibiting significant variations in fracture aperture (Figure 5c,d,i). In addition, dissolved tectonic fractures can form through dissolution after the initial formation of tectonic fractures (Figures 5d and 6).

4.2. Characteristics of Natural Fractures

The fractures observed in the study area predominantly consist of shear fractures. Notable variations exist in fracture density among different types of natural fractures (Figure 6). A statistical analysis of shear fracture density based on core samples and image logs found that the average fracture density can reach 9.7 m^{-1}. Conversely, the average density of tensile fractures is a mere 0.05 m^{-1}. Additionally, the average fracture density for bedding fractures is 0.94 m^{-1} and for stylolites it is 0.7 m^{-1}. Dissolution fractures exhibit a relatively lower density at 0.65 m^{-1}. Consequently, this study primarily concentrates on the statistical analysis of the strike, dip angle, and filling conditions of tectonic shear fractures.

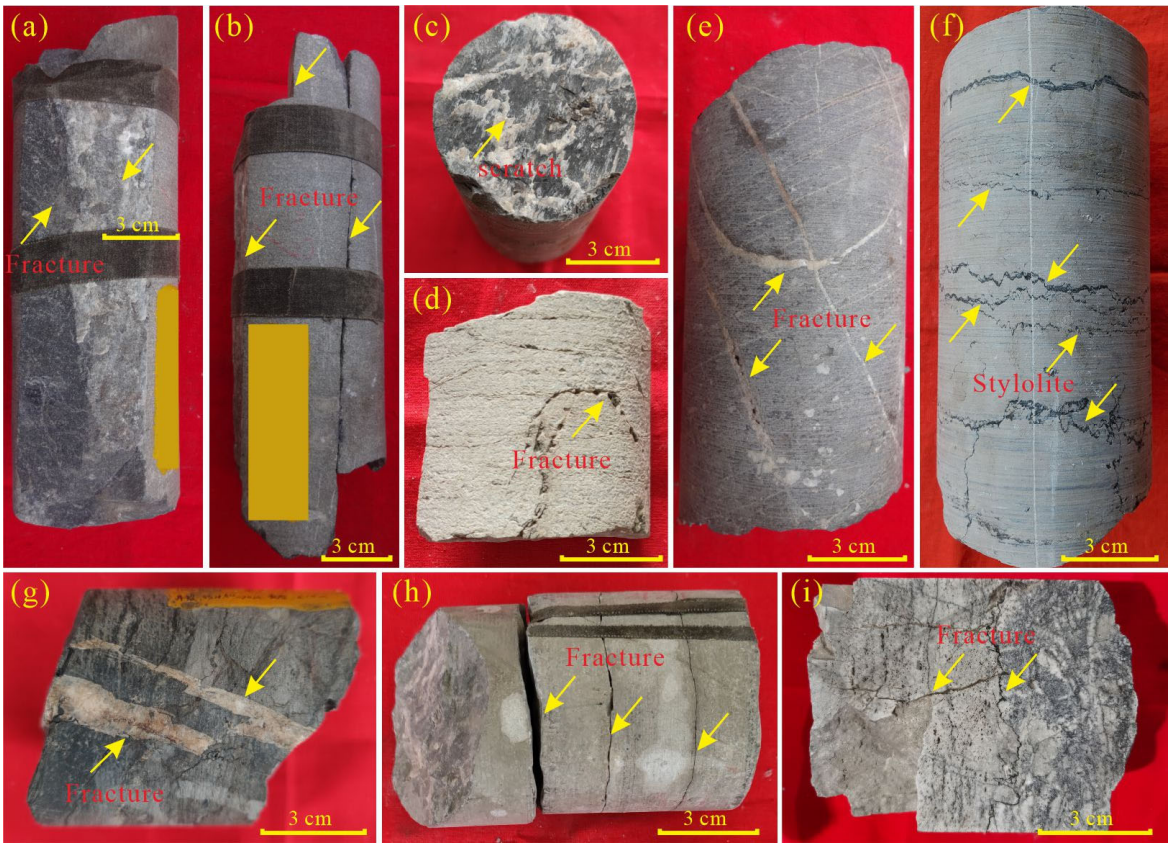

Figure 4. Characteristics of different types of natural fractures in cores of the Feixianguan Formation. (**a**) Two groups of sub-vertical tectonic shear fractures, well HL 004-2, 3477.85 m. (**b**) En echelon tectonic fractures, well PS1, 2792.17 m. (**c**) Shear fracture with scratches, well P3, 3557.30 m. (**d**) Dissolved tectonic fracture, well PD1, 5177.36 m. (**e**) Conjugated sub-vertical shear fractures, well LJ5, 2958.17 m. (**f**) Horizonal zigzag stylolites, well DS1, 6131.83 m. (**g**) Tensile fractures with uneven fracture plane and variable width, well P3, 3421.50 m. (**h**) Horizontal bedding fractures with evenly spaced intervals, well P1, 3441.90 m. (**i**) Sub-vertical tectonic shear fractures were cut by stylolite, well PG2, 3690.34 m.

The Feixianguan Formation in the study area exhibits extensive development of shear fractures, commonly occurring in clusters. Analysis of these fractures using image logs shows various strike directions, including NEE–SWW, NW–SE, NE–SW, and near E–W orientations. The NEE–SWW direction is the most prevalent (Figure 7a).

Based on their dip angle, fractures in the Feixianguan Formation can be classified into five categories: near-vertical fractures (>80°), high-angle fractures (60–80°), medium-angle fractures (30–60°), low-angle fractures (10–30°), and near-horizontal fractures (<10°). The majority of fractures, accounting for 52% of the total, exhibit dip angles in the range of 60–90°. Medium-angle fractures (30–60°) comprise approximately 25% of the fractures.

Low-angle fractures (10–30°) and near-horizontal fractures (<10°) account for the remaining 23% (Figure 7b).

The statistical analysis of the fill ratio of shear fractures revealed that 60% of the fractures were unfilled, while the remaining 40% were filled. The fractures in the study area were filled with various materials (Figure 8). Calcite was the dominant filling material among the fractures, accounting for 74%. Other filling materials included bitumen organic matter, terrigenous mud, dolomite, quartz, and gypsum (Figure 8). It is worth noting that some fractures exhibited multiple filling materials. For instance, in a calcite-filled fracture, the calcite and fracture wall edges were contaminated by bitumen (Figure 9a).

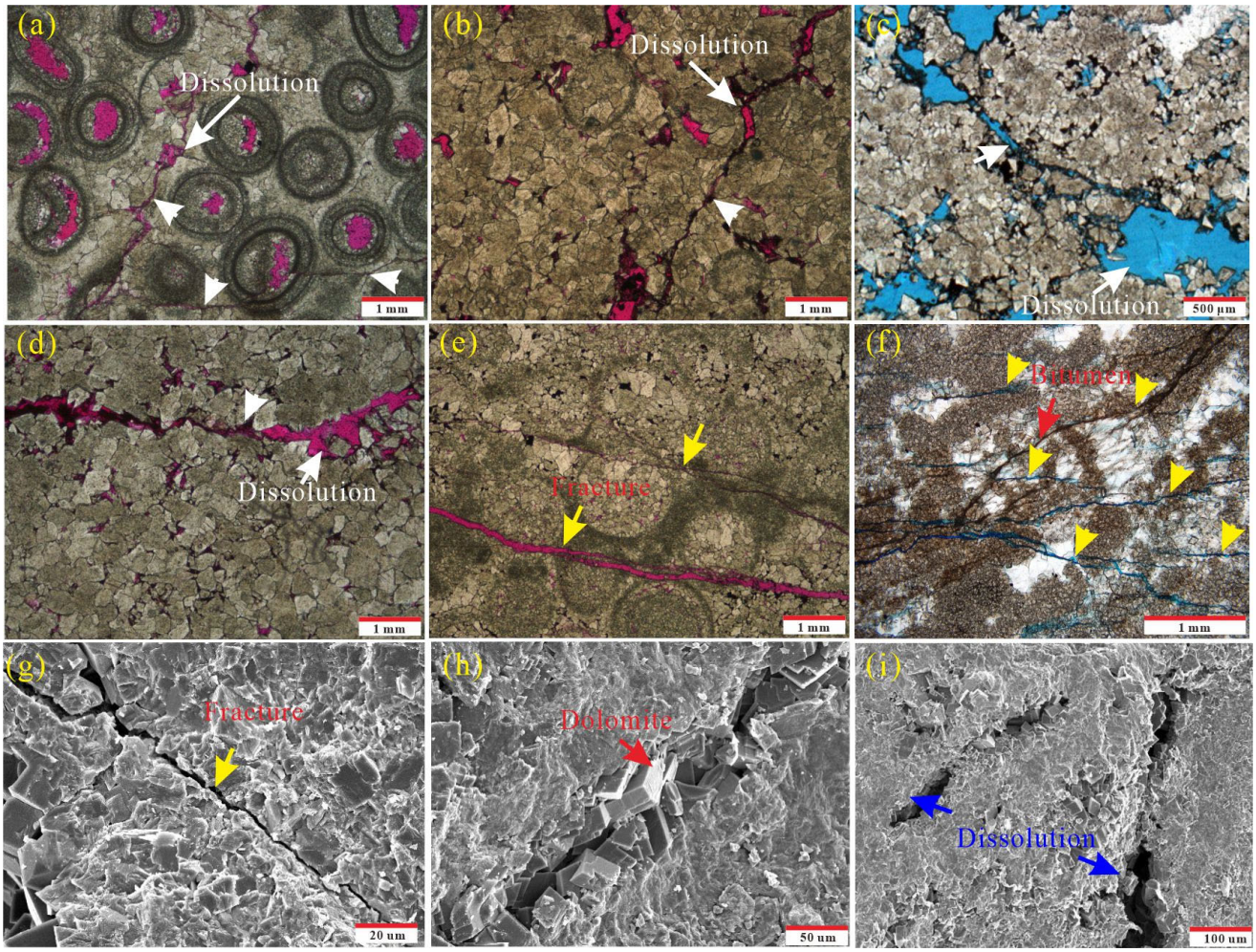

Figure 5. Characteristics of natural fractures in thin sections and SEM. (**a**) Intra-grain pores and dissolved tectonic fracture, well PG104, 5784.05 m, thin section with red casting. (**b**) Dissolved tectonic fracture is partially filled with bitumen, well PG104, 5796.48 m, thin section with red casting. (**c**) Connected dissolution pores form dissolution fracture, well PG304, 5555.42 m, thin section with blue casting. (**d**) Tectonic fracture expands dissolution pores, well PG104, 5793.4 m, thin section with red casting. (**e**) Two nearly parallel dissolved tectonic fractures, well PG104, 5672.13 m, thin section with red casting. (**f**) Multiple tectonic fractures form fracture networks, well P1, 3429.62 m, thin section with blue casting. (**g**) Tectonic micro-fractures, well PG104, 56,709.02 m. (**h**) Dolomite-filled tectonic micro-fracture, well PG104, 56,716.13 m. (**i**) Two sets of dissolved tectonic micro-fractures, well PG104, 56716.15 m.

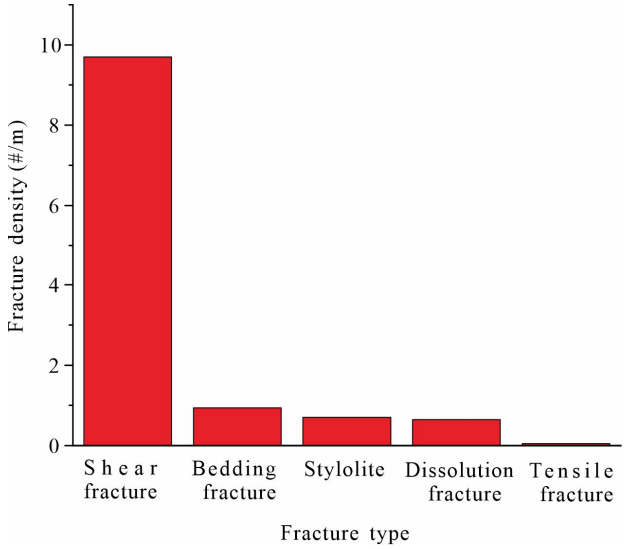

Figure 6. The average density of different types of fractures.

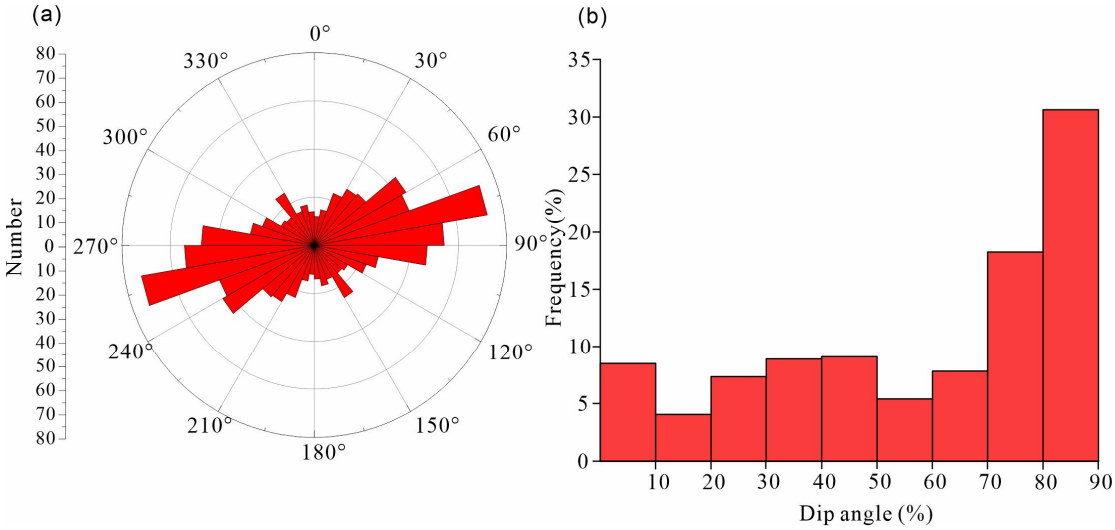

Figure 7. The distribution of tectonic fracture occurrence. (**a**) Strike rose diagram of the tectonic fractures in the study area from borehole image logs (N = 521). (**b**) Histograms of the tectonic shear fracture dip angle from cores and borehole image logs (N = 2508).

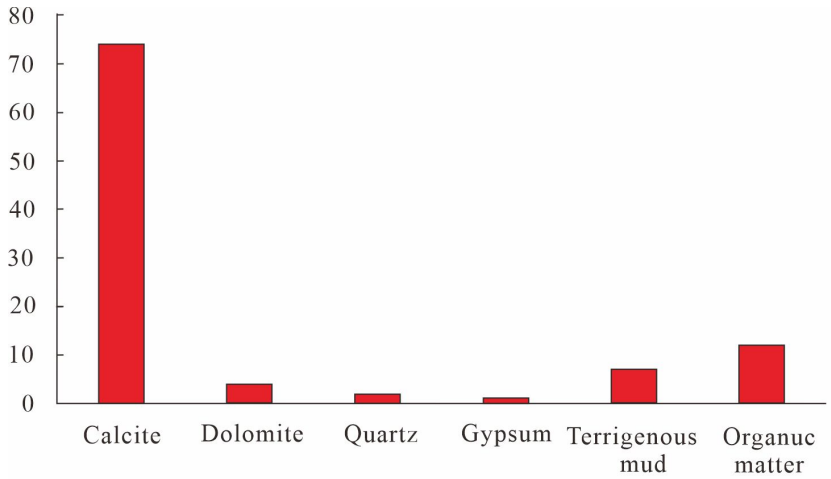

Figure 8. The proportion of different types of fillings in the tectonic fractures.

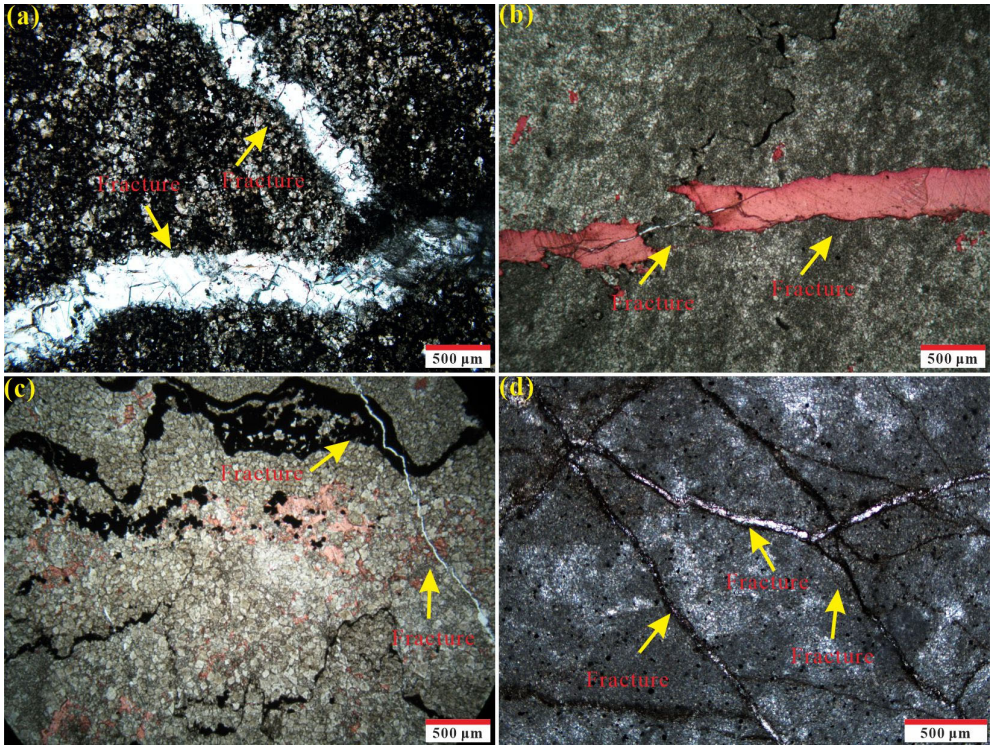

Figure 9. The cross-cutting relationship of different stages of fractures in the thin sections. (**a**) Micritic dolomite with two generations of tectonic fractures filled by calcite, the early vein terminates at the later, some calcite crystals are contaminated by bitumen, well P1, 5457.35 m. (**b**) The unfilled tectonic fractures cut a tectonic fracture filled with calcite, well PG102, 5582.96 m, stained by alizarin red. (**c**) Calcite-filled tectonic fractures cross-cut bitumen-filled fractures, well PG102, 5623.15 m. (**d**) Calcite-filled tectonic fractures cross-cut bitumen-filled fractures, well PG2, 4483.84 m.

4.3. Timing of Tectonic Fractures

To determine the sequence of fractures, it is essential to analyze the cross-cutting relationships between fractures. The timing of fracture formation can be inferred based on the cross-cutting relationships. By analyzing the fracture filling degree and their relationships to other fractures, we can determine the relative timing of fracture formation within the Feixianguan Formation.

At least two phases of calcite cementation can be identified based on the degree of contamination of calcite minerals in fractures. The Feixianguan Formation underwent the formation and cracking stages of paleo oil reservoirs, which led to the susceptibility of early calcite cement to bitumen contamination. As a result, these early calcite cements exhibit muddy crystal faces. On the other hand, the late calcite cements that filled the fractures appear clean (Figure 9a) because their formation occurred after the oil cracking process. For instance, as depicted in Figure 9a, the bitumen residue distributed in the gaps of calcite crystals indicates that this fracture was formed before bitumen charging. Furthermore, the early calcite-filled fractures were penetrated by late fractures filled with black bitumen (Figure 9a).

The fracture filled with clean calcite terminates in the fracture filled with bitumen, suggesting that the formation of clean calcite occurred after the formation of the bitumen-filled fracture (Figure 9c,d). The unfilled fractures intersect with the clean calcite veins (Figure 9b), indicating that these unfilled fractures were formed after the late-stage clean calcite filling. At least three periods of tectonic fractures were identified in this study by analyzing fracture-filling characteristics and cross-cutting relationships.

Given that the cement precipitated during the initial stages of fracture opening, the homogenization temperature of fluid inclusions within the cement can be used as a proxy to determine the timing of fracture formation. Integrating this information with the burial

history and thermal evolution can establish the sequence and duration of fracture formation. The microthermometric analysis of fluid inclusions within the fracture-filling minerals revealed three distinct intervals of homogenization temperatures (Figure 10). Three corresponding stages of tectonic events were identified based on the burial history and paleo-temperature conditions. The fluid inclusions of Stage I display a temperature range of 90 °C to 130 °C, with a concentration primarily between 100 °C and 110 °C. These temperatures correspond to the Late Indosinian to Early Yanshanian period. During this stage, the density of fluid inclusions is relatively low, indicating a limited degree of crystallization during the early diagenetic phase. In Stage II, the fluid inclusions display a more comprehensive temperature range from 170 °C to 205 °C. This temperature range corresponds to the Late Jurassic to the Cretaceous period, specifically the Late Yanshanian to Early Himalayan period, representing a significant burial depth period. In Stage III, the fluid inclusions exhibit temperatures ranging from 130 °C to 150 °C. These temperatures are representative of the Late Himalayan period, characterized by tectonic uplift (Figure 10).

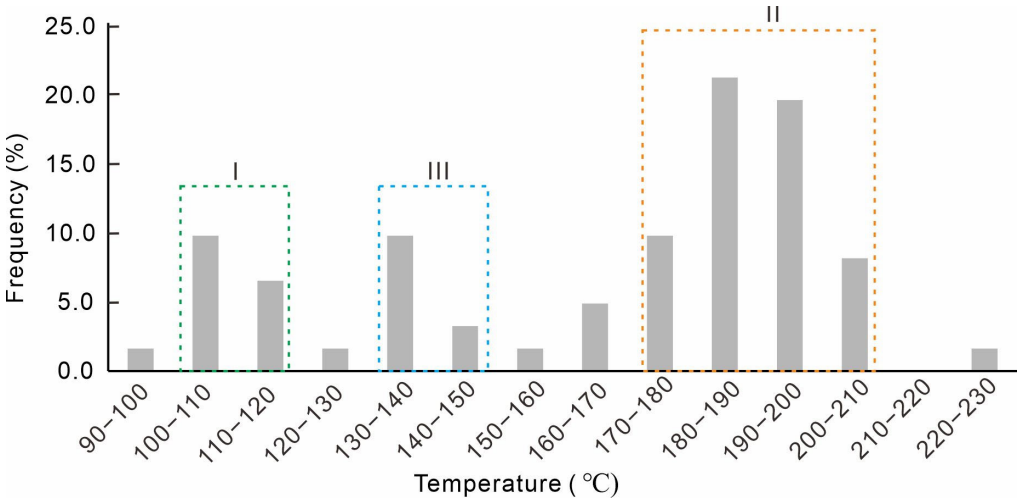

Figure 10. A histogram of the homogenization temperatures of inclusions in calcite veins (N = 72). I represents the Stage I fractures. II represents the Stage II fractures. III represents the Stage III fractures.

5. Discussion

5.1. Effectiveness of Natural Fractures

The degree of fracture filling is a crucial parameter for assessing fracture efficiency. The conditions of fracture filling are intricately associated with factors such as the time of formation, fluid dynamics, and the in situ stress field [11,43]. Unfilled tectonic fractures are predominantly oriented in the NEE–SWW and NE–SW directions (Figure 11a). Mineral-filled fractures predominantly exhibit strikes near E–W, NEE–SSW, and NNW–SSE (Figure 11b). The proportion of mineral-filled fractures with strikes in the NW–SE, NNW–SSE, and near S–N directions is relatively high. In contrast, the proportion of mineral-filled fractures in the NEE–SWW, NE–SW, and near E–W directions is low (Figure 11c). This suggests that the NEE–SWW, NNE–SSW, and near E–W directions exhibit many effective fractures.

During the Indonesian and Yanshanian periods, fractures experienced early formation, rendering them more prone to long-term fluid–rock interactions and subsequent mineral filling. Notably, the fractures striking NW–SE, which formed during the Indonesian period, and those striking near N–S, which formed during the late Yanshanian period, exhibited relatively high filling proportions. Conversely, the near NEE–SWW-striking fractures that developed during the late Himalayan period displayed a low filling proportion (Figure 11).

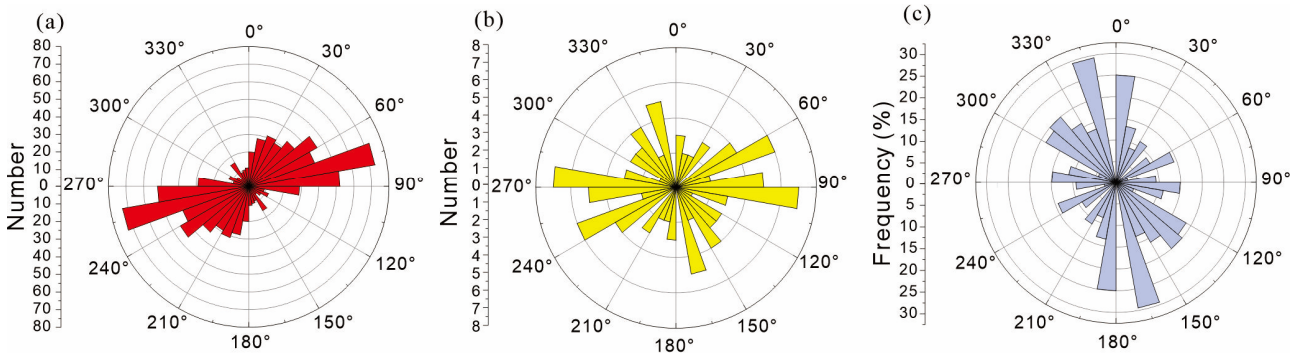

Figure 11. Filling degree of tectonic fractures with different strikes. (**a**) Strike rose diagram of unfilled tectonic fractures obtained from borehole image logs (N = 466). (**b**) Strike rose diagram of mineral-filled fractures obtained from image logs (N = 55). (**c**) Proportion of filling fractures with different strikes obtained from image logs (N = 521).

Our observations indicate that in situ stress significantly influences fracture effectiveness. The determination of in situ stress directions can be achieved through the analysis of induced fractures. Image logs of the Feixianguan Formation in our study area reveal that induced fractures often display echelon patterns in a double-row arrangement (Figure 12a). Specifically, induced fractures aligned in the NEE–SWW direction suggest that the in situ stress direction is NEE–SWW (Figure 12b). We further observed that fractures intersecting the in situ stress direction at a small angle, specifically in the NEE–SWW, NNE–SSW, and near E–W directions, are highly efficient (Figure 11).

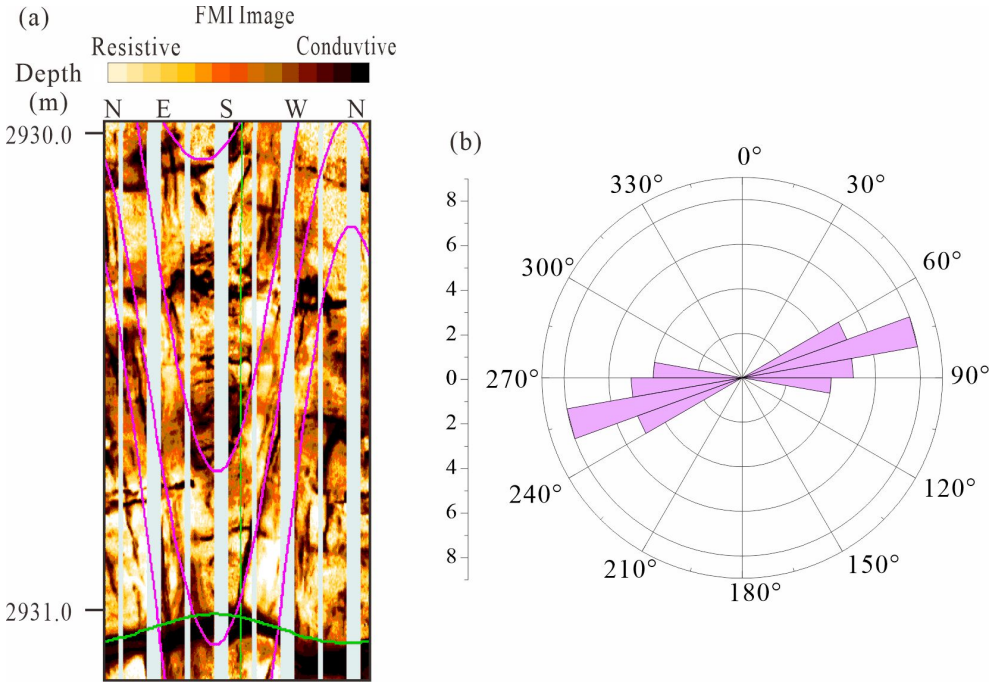

Figure 12. Characteristics of induced fractures of the Feixianguan Formation. (**a**) Drilling-induced fractures are en-echelon fractures inclined relative to the borehole axis, well L5. Solid purple lines represent fractures in interpretation. The solid green line represents the stratigraphic interface. (**b**) The strike rose diagram of drilling-induced fractures derived from image logs of 4 wells (N = 22).

5.2. Influence on Gas Migration and Accumulation

Intense tectonic activity can cause changes in the tectonic stress field, which in turn can alter the pressure of pore fluids within rocks. This change can affect the pressure gradient of the pore fluids, inducing fluid flow within the rock. However, in sealed reservoirs, an

increase in fluid pressure alone may not be sufficient to drive the migration of fluids such as oil and gas [44,45]. Tectonic fractures facilitate fluid flow within rocks by serving as storage spaces and conduits [12,46]. Specifically, elongated tectonic fractures can experience dissolution on their surfaces when exposed to acidic fluids during later stages, further enhancing the reservoir properties. This study focuses on the sedimentation of well-developed shoal facies carbonate rocks in the Feixianguan Formation. Shoal bodies, which include intra-platform and platform margin shoals, possess superior reservoir properties. They serve as the primary accumulation areas for oil and gas.

Previous research has extensively investigated the characteristics of petroleum accumulation in the Feixianguan Formation. Based on the analysis of burial history in the study area, it has been established that the Feixianguan Formation underwent two distinct periods of oil and gas charge and accumulation [27]. The first period occurred during the late Indosinian to early Yanshanian periods when liquid petroleum migrated and accumulated in the reservoirs. This process of migration and accumulation resulted in the formation of fluid oil reservoirs. The second period occurred during the deep burial stage of the Yanshanian period. During this phase, the liquid oil in the reservoirs underwent thermal cracking, transforming it into gas; consequently, bitumen residues were formed. Subsequently, during the late Yanshanian to Himalayan periods, structural-lithologic gas reservoirs were formed due to degassing that accompanied the uplift process (Figure 13). This degassing process contributed to the accumulation of gas in the reservoirs.

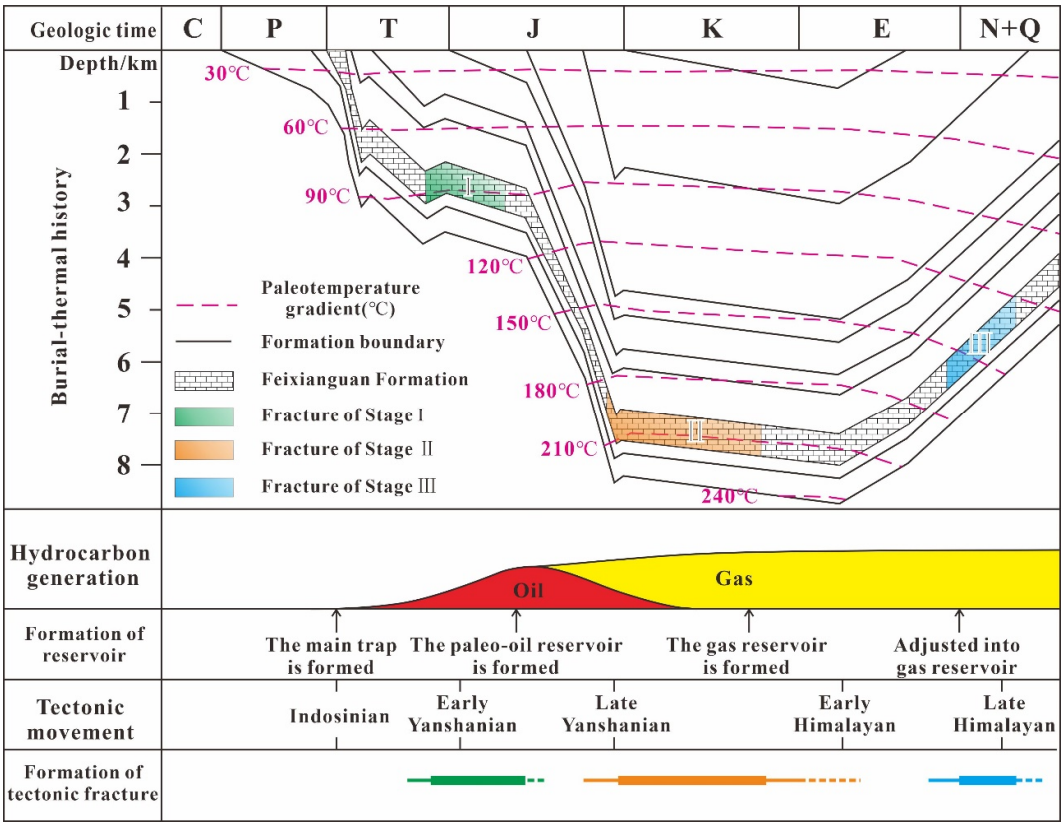

Figure 13. The relationship between oil and gas charging and tectonic fracture formation time of Feixianguan Formation in the study area.

According to the burial history and petroleum accumulation model of the Feixianguan Formation, the initial fractures (stage I) originated during the Middle Triassic period, specifically from the late Indosinian to early Yanshanian periods (Figure 13). It is worth noting that many of these fractures were filled with minerals such as calcite (Figure 9a). These fractures either pre-date or were formed contemporaneously with the petroleum accumulation period. Intense tectonic activities, as documented by Li et al. (2021) [35], occurred

during the late Yanshanian period, leading to the formation of stage II fractures (Figure 13). These fractures provided storage space for oil and gas and facilitated the migration of hydrocarbons and other diagenetic fluids. Subsequently, during the Himalayan period, changes in the tectonic stress field led to the development of a series of NE–SW and nearly E–W-striking fractures (stage III) within the reservoir rocks (Figure 13). In conjunction with the pre-existing fractures, these fractures interconnected and intersected, forming an open and connected fracture network within the reservoir (Figure 5f). This fracture network played a crucial role in enhancing the productivity of carbonate oil and gas reservoirs. It is noteworthy that the filling degree of the fractures formed during the Himalayan period was relatively low. These fractures, coinciding with the uplift and degassing phase of the oil and gas deposits, served as migration pathways for oil and gas and provided storage space for natural gas. The presence of residual bitumen in the carbonate fractures of the Feixianguan Formation, as observed in the thin sections, further supports this perspective (Figure 9a,c).

The Feixianguan Formation has undergone multiple phases of tectonic activities, forming fractures with diverse orientations due to shifts in the tectonic stress field. These fractures, formed at different stages, have subsequently intersected and interconnected, thereby creating a network of fractures that facilitate the migration and accumulation of oil and gas. The flow of dissolution fluids has further enhanced the permeability of these fractures. Notably, the tectonically controlled fractures from the late Yanshanian and Himalayan periods have played a crucial role in the migration and storage of hydrocarbons in conjunction with petroleum accumulation events (Figure 13).

5.3. Contribution of Natural Fractures to Productivity

Previous studies have indicated that the impact of natural fractures on productivity is primarily manifested in aspects such as fracture density, effective fracture density, fracture orientation, and fracture aperture [47]. Our initial analysis focuses on the relationship between fracture density and production. The productivity of individual wells in the study area, specifically those in the Feixianguan Formation reservoirs, displays significant variability. Interestingly, our findings reveal that the gas production of a single well does not strongly correlate with the total fracture density (Figure 14a), suggesting that factors other than the total fracture density exert a more significant influence on gas production. However, our findings indicate a close relationship between the proportion of effective fractures and production. We observed no significant correlation between the proportion of effective fractures and production when the proportion of effective fractures is less than 42%. A notable positive correlation emerges between the proportion of effective fractures and the gas production of individual wells when the proportion of effective fractures exceeds 42%. As the proportion of effective fractures increases, there is an overall upward trend in the productivity of single wells (Figure 14b). This phenomenon could be attributed to the greatly improved connectivity of the fracture network when the effective fracture ratio exceeds 42%, thereby enhancing natural gas production. This finding highlights that the proportion of effective fractures rather than fracture density increases gas production.

A comparative analysis of fracture orientations from high-yielding and low-yielding wells reveals that fractures oriented in the NE–SW and NEE–SWW directions yield higher single-well natural gas production. Conversely, natural fracture production is low in the near N–S and NW–SE directions. This finding suggests that fractures oriented in the NE–SW and NEE–SWW directions are more effective in gas production (Figure 15). Mineral-filled fractures striking the NEE–SWW and NE–SW directions exhibit significant characteristics, although they account for a low proportion of the total fractures. These fractures, nearly parallel to the in situ stress of NEE–SWW, have larger apertures and are more effective than fractures with other strike directions. In the study area, the NE–SW- and NEE–SWW-striking fractures with relatively good effectiveness play a crucial role in the high single-well natural gas production. This suggests that these fractures intersect

with the current in situ stress at a small angle and can enhance gas production in the study area (Figure 15).

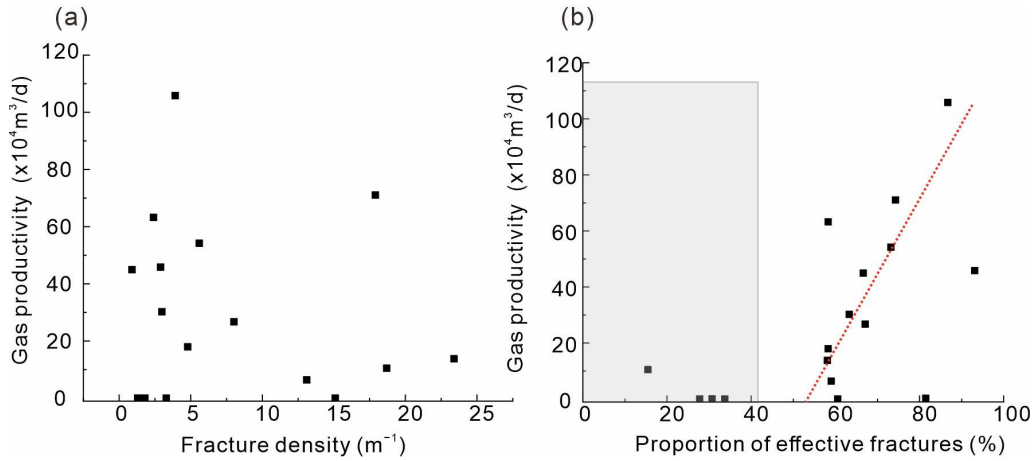

Figure 14. The influence of fracture density and proportion of effective fracture on oil and gas production in the Feixianguan Formation of the study area. (**a**) Correlation between fracture density and gas production: the data were obtained from 17 wells. (**b**) Correlation between the proportion of effective fractures and gas production: the data were obtained from 17 wells. The grey area represents effective fractures have no obvious correlation with natural gas productivity. The red dashed line indicates that effective fractures have a good correlation with natural gas productivity.

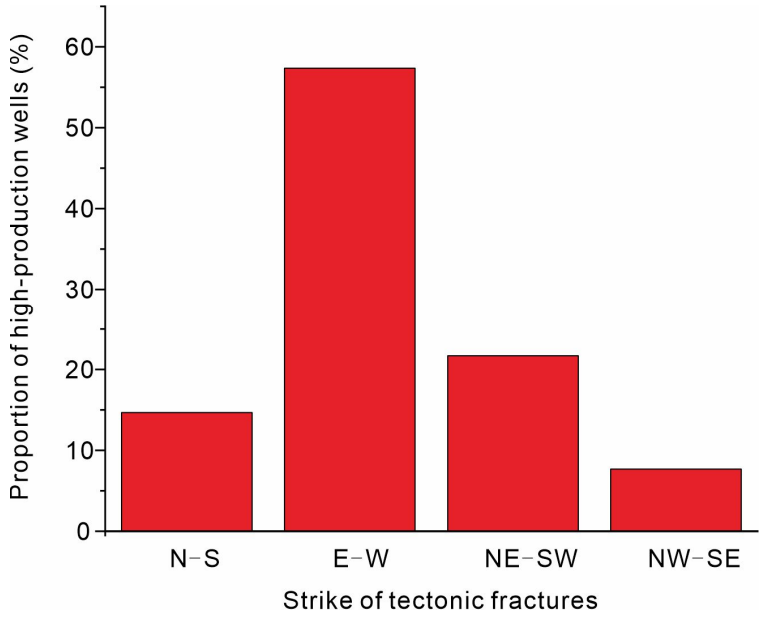

Figure 15. The relationship between the proportion of high-production wells and the strike of effective tectonic fractures.

6. Conclusions

The Feixianguan Formation, located in northeastern Sichuan, China, exhibits two types of fractures: tectonic and diagenetic. Among these, shear fractures are the most prominent, surpassing extensional, stylolites, bedding, and diagenetic fractures. The shear fractures predominantly display a NEE–SWW strike direction and a dip angle greater than 60°. Approximately 60% of the shear fractures remain unfilled, while the remaining fractures are filled with various materials. Calcite is the primary filling material, followed by bitumen organic matter, terrigenous mud, dolomite, quartz, and gypsum.

The fractures in the Feixianguan Formation can be classified into three main stages of formation. The first stage took place during the Late Indosinian–Early Yanshanian period, the second stage during the Late Yanshanian–Early Himalayan period, and the third stage during the Late Himalayan period. Among these fractures, the near N–S-striking fractures and NW–SE-striking fractures have a relatively high filling proportion, while the nearly E–W- and NEE–SWW-striking fractures have a low filling proportion. Fractures in the NEE–SWW, NNE–SSW, and near E–W directions intersect with the in situ stress direction at a small angle and exhibit good efficiency.

The initial fractures, primarily filled with minerals, formed either before or concurrently with the creation of the oil reservoirs. Subsequently, the secondary fractures emerged, serving as both storage areas and conduits for the migration of oil and gas. These secondary fractures played a crucial role in facilitating the movement of hydrocarbons. The tertiary fractures, which contained fewer filling minerals, corresponded to the phase of reservoir adjustment characterized by uplift and gas release. The accumulation and interconnection of fractures from various stages gave rise to a fracture network, which served as migration pathways for oil and gas and storage spaces within the reservoir.

In controlling gas production, the density of fractures, particularly effective fractures, plays a crucial role. An increase in the proportion of effective fractures leads to an overall improvement in single-well productivity. Moreover, the orientation of these effective fractures also significantly impacts natural gas production. Fractures striking in the NE–SW and NEE–SWW directions, demonstrating relatively good effectiveness, are associated with high levels of single-well natural gas production. These observations highlight the importance of considering effective fracture density and orientation when analyzing and optimizing gas production.

Author Contributions: Conceptualization, C.G.; Methodology, C.G. and Y.Y.; Formal analysis, C.G. and Y.Y.; Investigation, C.G., Y.Y. and D.L.; Resources, H.Z. and J.Z.; Writing—original draft, C.G. and Y.Y.; Writing—review & editing, C.G.; Visualization, D.L.; Supervision, L.Z.; Project administration, L.Z.; Funding acquisition, L.Z. All authors have read and agreed to the published version of the manuscript.

Funding: This paper is supported by the National Natural Science Foundation of China (No. U21B2062).

Institutional Review Board Statement: Not applicable.

Informed Consent Statement: Not applicable.

Data Availability Statement: Data are contained within the article.

Acknowledgments: The authors highly appreciate the information and support from the Northeastern Sichuan Oil and Gas District, PetroChina Southwest Oil and Gas Field Company. We thank the editor and several anonymous reviewers for their constructive comments, which have significantly contributed to improving this article.

Conflicts of Interest: Authors Hang Zhang and Jiewei Zhang were employed by the Northeastern Sichuan Oil and Gas District, PetroChina Southwest Oil and Gas Field Company. The remaining authors declare that the research was conducted in the absence of any commercial or financial relationships that could be construed as a potential conflict of interest.

References

1. Garland, J.; Neilson, J.; Laubach, S.E.; Whidden, K.J. Advances in carbonate exploration and reservoir analysis. *Geol. Soc. Spec. Publ.* **2012**, *370*, 1–15. [CrossRef]
2. Lucia, F.J.; Kerans, C.; Jennings, J.J.W. Carbonate reservoir characterization. *J. Pet. Technol.* **2003**, *55*, 70–72. [CrossRef]
3. Moore, C.H.; Wade, W.J. *Carbonate Reservoirs: Porosity and Diagenesis in a Sequence Stratigraphic Framework*; Elsevier: Amsterdam, The Netherlands, 2013; p. 67.
4. Roehl, P.O.; Choquette, P.W. Perspectives on world-class carbonate petroleum reservoirs. *Am. Assoc. Pet. Geol. Bull.* **1985**, *69*, 148.
5. Lavenu, A.P.C.; Lamarche, J.; Gallois, A.; Gauthier, B.D.M. Tectonic versus diagenetic origin of fractures in a naturally fractured carbonate reservoir analog (Nerthe anticline, southeastern France). *Am. Assoc. Pet. Geol. Bull.* **2013**, *97*, 2207–2232. [CrossRef]

6. Lorenz, J.C.; Farrell, H.E.; Hanks, C.L.; Rizer, W.D.; Sonnenfeld, M.D. Carbonate seismology: Characteristics of natural fractures in carbonate strata. *Soc. Explor. Geophys. Geophys. Dev. Ser.* **1997**, *6*, 197–202.
7. Wennberg, O.P.; Casini, G.; Jonoud, S.; Peacock, D. The characteristics of open fractures in carbonate reservoirs and their impact on fluid flow, a discussion. *Pet. Geosci.* **2016**, *22*, 91–104. [CrossRef]
8. Finkbeiner, T.; Barton, C.A.; Zoback, M.D. Relationships among in-situ stress, fractures and faults, and fluid flow, Monterey Formation, Santa Maria Basin, California. *Am. Assoc. Pet. Geol. Bull.* **1997**, *81*, 1975–1999.
9. Zeng, L.B.; Tang, X.M.; Wang, T.C.; Gong, L. The influence of fracture cements in tight Paleogene saline lacustrine carbonate reservoirs, western Qaidam Basin, northwest China. *Am. Assoc. Pet. Geol. Bull.* **2012**, *96*, 2003–2017. [CrossRef]
10. Hollis, C.; Vahrenkamp, V.; Tull, S.; Mookerjee, A.; Taberner, C.; Huang, Y.D. Pore system characterisation in heterogeneous carbonates, An alternative approach to widely-used rock-typing methodologies. *Mar. Pet. Geol.* **2010**, *27*, 772–793. [CrossRef]
11. Laubach, S.E.; Eichhubl, P.; Hilgers, C.; Lander, R. Structural diagenesis. *J. Struct. Geol.* **2010**, *32*, 1866–1872. [CrossRef]
12. Antonellini, M.; Mollema, P.N. A natural analog for a fractured and faulted reservoir in dolomite; Triassic Sella Group, northern Italy. *Am. Assoc. Pet. Geol. Bull.* **2000**, *84*, 314–344.
13. Sagi, D.A.; De Paola, N.; McCaffrey, K.J.W.; Holdsworth, R.E. Fault and fracture patterns in low porosity chalk and their potential influence on sub-surface fluid flow—A case study from Flamborough Head, UK. *Tectonophysics* **2016**, *690*, 35–51. [CrossRef]
14. Barton, C.; Moos, D.; Tezuka, K. Geomechanical wellbore imaging, Implications for reservoir fracture permeability. *Am. Assoc. Pet. Geol. Bull.* **2009**, *93*, 1551–1569. [CrossRef]
15. Hennings, P.; Allwardt, P.; Paul, P.; Zahm, C.; Reid, R.; Alley, H.; Kirschner, R.; Lee, B.; Hough, E. Relationship between fractures, fault zones, stress, and reservoir productivity in the Suban gas field, Sumatra, IndonesiaSuban Gas Field, Sumatra, Indonesia. *Am. Assoc. Pet. Geol. Bull.* **2012**, *96*, 753–772.
16. Wang, Z.; Lü, X.X.; Wang, S.; Li, Y.; Zhou, X.X.; Quan, H.; Li, R.B. Fracture systems and petrophysical properties of tight sandstone undergoing regional folding, A case study of the Cretaceous reservoirs in the Kuqa foreland thrust belt, Tarim Basin. *Mar. Pet. Geol.* **2020**, *112*, 104055. [CrossRef]
17. Gudmundsson, A.; Simmenes, T.H.; Larsen, B.; Philipp, S.L. Effects of internal structure and local stresses on fracture propagation, deflection, and arrest in fault zones. *J. Struct. Geol.* **2010**, *32*, 1643–1655. [CrossRef]
18. Jeanne, P.; Guglielmi, Y.; Lamarche, J.; Cappa, F.; Marié, L. Architectural characteristics and petrophysical properties evolution of a strike-slip fault zone in a fractured porous carbonate reservoir. *J. Struct. Geol.* **2012**, *44*, 93–109. [CrossRef]
19. Yao, Y.T.; Zeng, L.B.; Mao, Z.; Han, J.; Cao, D.S.; Lin, B. Differential deformation of a strike-slip fault in the Paleozoic carbonate reservoirs of the Tarim Basin, China. *J. Struct. Geol.* **2023**, *173*, 104908. [CrossRef]
20. Fan, X.J.; Peng, J.; Li, J.X.; Chen, D.; Li, F.; Deng, J.H.; Miao, Z.W. Fracture characteristics of ultra-deep reef-bank lithologic gas reservoirs in the Upper Permian Changxing Formation in Yuanba area, northeastern Sichuan Basin. *Oil Gas Geol.* **2014**, *35*, 511–516. (In Chinese with English Abstract)
21. Jiang, L.; Worden, R.H.; Cai, C.F.; Shen, A.J.; He, X.Y.; Pan, L.Y. Contrasting diagenetic evolution patterns of platform margin limestones and dolostones in the Lower Triassic Feixianguan Formation, Sichuan Basin, China. *Mar. Pet. Geol.* **2018**, *92*, 332–351. [CrossRef]
22. Guo, X.S.; Hu, D.F.; Li, Y.P.; Duan, J.B.; Ji, C.H.; Duan, H. Discovery and theoretical and technical innovations of Yuanba gas field in Sichuan Basin, SW China. *Pet. Explor.* **2018**, *45*, 15–28. [CrossRef]
23. Ma, X.H.; Yang, Y.; Wen, L.; Luo, B. Distribution and exploration direction of medium- and large-sized marine carbonate gas fields in Sichuan Basin, SW China. *Pet. Explor.* **2019**, *46*, 1–15. [CrossRef]
24. Jiang, L.; Worden, R.H.; Cai, C.F.; Li, K.K.; Xiang, L.; Cai, L.L.; He, X.Y. Dolomitization of gas reservoirs, the upper Permian Changxing and lower Triassic Feixianguan Formations, Northeast Sichuan Basin, China. *J. Sediment. Res.* **2014**, *84*, 792–815. [CrossRef]
25. Huo, F.; Wang, X.Z.; Wen, H.G.; Xu, W.L.; Huang, H.W.; Jiang, H.C.; Li, Y.W.; Li, B. Genetic mechanism and pore evolution in high quality dolomite reservoirs of the Changxing-Feixianguan Formation in the northeastern Sichuan Basin, China. *J. Pet. Sci. Eng.* **2020**, *194*, 107511. [CrossRef]
26. Ma, Y.S.; Guo, X.S.; Guo, T.L.; Huang, R.; Cai, X.Y.; Li, G.X. The Puguang gas field, New giant discovery in the mature Sichuan Basin, southwest China. *Am. Assoc. Pet. Geol. Bull.* **2007**, *91*, 627–643. [CrossRef]
27. Ma, Y.S.; Cai, X.X.; Li, G.X. Basic characteristics and concentration of the Puguang Gas Field in the Sichuan Basin. *Acta Geol. Sin.* **2005**, *79*, 858–865. (In Chinese with English Abstract)
28. Ding, X.; Wu, H.; Sun, Y.F.; Yu, H.H.; Zhao, Z.H.; Chen, J.S.; Tang, Q.S. Genetic types of carbonate shoal reservoirs in the Middle Triassic of the Sichuan Basin (SW China). *Mar. Pet. Geol.* **2019**, *99*, 61–74. [CrossRef]
29. Tan, X.C.; Liu, H.; Li, L.; Luo, B.; Liu, X.G.; Mou, X.H.; Nie, Y.; Xi, W.Y. Primary intergranular pores in oolitic shoal reservoir of lower triassic feixianguan formation, Sichuan Basin, Southwest China, Fundamental for reservoir formation and retention diagenesis. *J. Earth Sci.* **2011**, *22*, 101–114. [CrossRef]
30. Shao, X.Z.; Qin, Q.R.; Fan, X.L.; Shi, L.C. Fracture prediction of the bottom of T_1f^4 in Huanglongchang structure, northeastern Sichuan Basin. *Lithol. Reserv.* **2011**, *23*, 96–100. (In Chinese with English Abstract)
31. Wang, Y.F.; Zhao, X.Y.; Liu, C.C. Development characteristics and main controlling factors of natural fractures in reef-flat facies reservoirs of Changxing Formation in Yuanba area, northeastern Sichuan Basin. *Nat. Gas Geosci.* **2019**, *30*, 973–981. (In Chinese with English Abstract)

32. Yao, Y.T.; Zeng, L.B.; Zhang, H.; Zhang, J.W.; Guan, C.; Liang, D. Fracture Development Laws of Feixianguan Formation Carbonate Reservoirs in Huanglongchang-Qilibei Area, Northeast Sichuan. *Earth Sci.* **2023**, *48*, 2643–2651.
33. Tang, H.; Wang, Q.L.; Peng, X.L.; Li, L.; Huang, D.M. The Study of Fracture Characteristics and Causes at Feixianguan Formation inXuanhan Area of Eastern Sichuan. *J. Southwest Pet. Univ. (Sci. Technol. Ed.)* **2011**, *33*, 78. (In Chinese with English Abstract)
34. Zhao, W.Z.; Luo, P.; Chen, G.S.; Cao, H.; Zhang, B.M. Origin and reservoir rock characteristics of dolostones in the Early Triassic Feixianguan Formation, NE Sichuan Basin, China, Significance for future gas exploration. *J. Pet. Geol.* **2005**, *28*, 83–100. [CrossRef]
35. Li, P.P.; Zou, H.Y.; Yu, X.Y.; Hao, F.; Wang, G.W. Source of dolomitizing fluids and dolomitization model of the upper Permian Changxing and Lower Triassic Feixianguan formations, NE Sichuan Basin, China. *Mar. Pet. Geol.* **2021**, *125*, 104834. [CrossRef]
36. Li, K.K.; George, S.C.; Cai, C.F.; Zhang, X.F.; Tan, X.F. Comparison of differential diagenesis of two oolites on the Lower Triassic platform margin, NE Sichuan Basin, Implications for the co-evolution of rock structure and porosity. *Mar. Pet. Geol.* **2020**, *119*, 104485. [CrossRef]
37. He, D.F.; Li, D.S.; Zhang, G.W.; Zhao, L.Z.; Fan, C.; Lu, R.Q.; Wen, Z. Formation and evolution of multi-cycle superposed Sichuan Basin, China. *Chin. J. Geol.* **2011**, *46*, 589–606. (In Chinese with English Abstract)
38. Laubach, S.E.; Olson, J.E.; Gross, M.R. Mechanical and fracture stratigraphy. *Am. Assoc. Pet. Geol. Bull.* **2009**, *93*, 1413–1426. [CrossRef]
39. Ortega, O.J.; Marrett, R.A.; Laubach, S.E. A scale-independent approach to fracture intensity and average spacing measurement. *Am. Assoc. Pet. Geol. Bull.* **2006**, *90*, 193–208. [CrossRef]
40. Dickson, J. A Modified Staining Technique for Carbonates in Thin Section. *Nature* **1965**, *205*, 587. [CrossRef]
41. Zhao, G.; Jin, Z.J.; Ding, W.L.; Liu, G.X.; Yun, J.B.; Wang, R.Y.; Wang, G.P. Developmental characteristics and formational stages of natural fractures in the Wufeng—Longmaxi Formation in the Sangzhi Block, Hunan Province, China: Insights from fracture cements and fluid inclusions studies. *J. Petrol. Sci. Eng.* **2022**, *208*, 109407. [CrossRef]
42. Goldstein, R.H.; Reynolds, T.J. *Systematics of Fluid Inclusions in Diagenetic Minerals*; SEPM Society for Sedimentary Geology: Tulsa, OK, USA, 1994.
43. Ravier, E.; Guiraud, M.; Guillien, A.; Vennin, E.; Buoncristiani, J.F.; Portier, E. Micro-to macro-scale internal structures, diagenesis and petrophysical evolution of injectite networks in the Vocontian Basin (France), Implications for fluid flow. *Mar. Pet. Geol.* **2015**, *64*, 125–151. [CrossRef]
44. Hantschel, T.; Kauerauf, A.I.; Wygrala, B. Finite element analysis and ray tracing modeling of petroleum migration. *Mar. Pet. Geol.* **2000**, *17*, 815–820. [CrossRef]
45. Wang, Y.; Song, Y.; Shan, J.Z. Action of tectonic stress on hydrocarbon migration and accumulation. *Oil Gas Geol.* **2005**, *26*, 563–571. (In Chinese with English Abstract)
46. Zeng, L.B.; Gong, L.; Guan, C.; Zhang, B.J.; Wang, Q.Q.; Zeng, Q.; Lyu, W.Y. Natural fractures and their contribution to tight gas conglomerate reservoirs, A case study in the northwestern Sichuan Basin, China. *J. Petrol. Sci. Eng.* **2022**, *210*, 110028. [CrossRef]
47. Wang, Y.Y.; Chen, J.F.; Pang, X.Q.; Liu, Y.F.; Chen, Z.Y.; Luo, G.P.; Zhang, G.Q.; Huang, L.M. Faulting controls on oil and gas composition in the Yingmai 2 Oilfield, Tarim Basin, NW China. *Org. Geochem.* **2018**, *123*, 48–66. [CrossRef]